Polymer 53 (2012) 3636–3641

Contents lists available at SciVerse ScienceDirect

Polymer

journal homepage: www.elsevier.com/locate/polymer

Blends of polyolefin/PMMA for improved scratch resistance, adhesion and compatibility

Jie Song [a,1], Christopher M. Thurber [a], Shingo Kobayashi [b,2], Adam M. Baker [a], Christopher W. Macosko [a,*], H. Craig Silvis [c]

[a] Department of Chemical Engineering and Materials Science, University of Minnesota, Minneapolis, MN 55455, USA
[b] Department of Chemistry, University of Minnesota, Minneapolis, MN 55455, USA
[c] Core R&D, 1776 Building, The Dow Chemical Company, Midland, MI 48674, USA

ARTICLE INFO

Article history:
Received 23 March 2012
Received in revised form
25 May 2012
Accepted 26 May 2012
Available online 7 June 2012

Keywords:
Blend
Adhesion
Compatibility

ABSTRACT

Functionalized poly(propylene-*co*-ethylene) (PPE) made via reactive extrusion dramatically improved the performance of their blends with poly(methyl methacrylate) (PMMA). Adhesion, compatibility, modulus, hardness and scratch resistance were all increased for blends with functional PPEs compared to non-modified PPE, greatly expanding the applications of polyolefins. Three types of functional PPEs including maleic anhydride grafted PPE (PPE-MA), hydroxyl group grafted PPE (PPE-OH) and secondary amine group grafted PPE (PPE-NHR) were melt blended with PMMA at different compositions and with PMMA of different molecular weights. Compatibility of each functional PPE with PMMA was compared by investigating the binary blends using mechanical (nano-indentation, nano-scratch and tensile tests), morphological (scanning electron microscopy with image analysis, particle size analysis) and adhesion tests. Compatibility of functional PPEs with PMMA is confirmed consistently from various tests and ranked in a decreasing order as follows: PPE-NHR > PPE-OH > PPE-MA > PPE. We also drastically improved the compatibility and adhesion between PPE and PMMA by blending a small amount of PMMA grafted PPE copolymer.

1. Introduction

Polyolefins are found in a variety of applications including food packaging, high strength fibers, building materials, and automotive exterior parts. Despite their wide usage, polyolefins suffer from relatively poor adhesion, low hardness and scratch resistance. In an effort to enhance the properties of polyolefins, e.g., adhesion [1–4], paintability, and impact strength, blends of polyolefins with polar polymers have received attention as an industrially relevant route over the past decades [5,6]. Polymer blends offer a means to achieve property combinations that are not generally available in any single polymeric material.

As polyolefins are not miscible with polar polymers, compatibilization is required to obtain maximum synergy by improving interfacial activity in heterogeneous polymer blends. Compatibilization can be achieved by adding a block or graft copolymer of the two polymer components in the blend or by forming such a copolymer through covalent or ionic bonds *in situ* during blending. The latter strategy is also known as reactive compatibilization.

This study investigated both reactive compatibilization and adding premade copolymers to generate compatibilized polyolefin/PMMA blends in order to improve polyolefin scratch resistance. The ability of polyolefin's surfaces to resist scratching is particularly important in coatings for automotives, building materials, and many other applications. PMMA is well known for its high mechanical strength, optical transparency, and excellent UV resistance, which makes it an excellent candidate for polyolefin scratch improvement.

Although some researchers have proposed the synthesis of PMMA-grafted polyolefins with controlled radical polymerization [7–9], the efficiency of these copolymers as compatibilizers has not been explored. While two reports indicate some improvement in the mechanical properties of polyolefins by blending with PMMA, very limited information is given regarding the properties of the products [10,11]. There are also no reports on reactive

* Corresponding author.
E-mail addresses: macosko@umn.edu, macosko@maroon.tc.umn.edu (C.W. Macosko).
[1] Present address: Dow Water & Process Solutions, 5250 W. 73rd street, Edina, MN 55439, USA.
[2] Present address: Department of Biochemical Engineering, Yamagata University, Japan.

0032-3861/$ – see front matter © 2012 Elsevier Ltd. All rights reserved.
http://dx.doi.org/10.1016/j.polymer.2012.05.057

compatibilization of polyolefins and PMMA. To our knowledge stabilized blends of PMMA with polyolefins have never been achieved.

We attacked the problem of compatibilizing such blends using both pre-made compatibilizers and reactive compatibilization. We show that blends made with these compatibilizers can significantly improve polyolefin scratch resistance and adhesion. This study will also illustrate the capabilities of a nanoindentation/nanoscratch tester to assess mechanical and tribological properties of polyolefins.

2. Experimental

2.1. Materials

Poly(propylene-*co*-ethylene) (VERSIFY™ 4301), PPE, was provided by The Dow Chemical Company. This copolymer has 11–12 wt% ethylene with a melt flow rate (MFR) of 25 g/10 min (230 °C; 2160 g) as measured by ASTM D 1238 and density of 0.868 g/cm^3 as measured by ASTM D 792. The anhydride-functionalized poly(propylene-*co*-ethylene) copolymer (PPE-MA) was prepared by free radical grafting of maleic anhydride onto another grade of poly(propylene-*co*-ethylene) copolymer (VERSIFY™ 2400) with 14–15 wt% ethylene in the melt using continuous reactive extrusion described in detail elsewhere. The anhydride content of PPE-MA was determined to be 0.80 wt% by a calibrated FT-IR analytical method. 0.80 wt% corresponds to about one succinic anhydride group per 1000 $-CH_2-$ units on the polyolefin backbone. The hydroxy- and amino-functional analogs were then prepared directly from PPE-MA by reactive extrusion with 2-aminoethanol and N-methyl-1,3-propanediamine as described by Silvis et al. [12].The relative concentrations of OH and NHR functionalities, N-(2-hydroxyethyl)-succinimide and N-(3-(N-methylamino)-1-propyl)-succinimide were 1.15 wt% and 1.36 wt%, respectively, based on complete conversion of the anhydride to functionalized imide as determined using FT-IR spectroscopy (anhydride C=O at 1790 cm^{-1}; imide C=O at 1705 cm^{-1}). Due to chain scission effects during maleation, the MFR increased to ~80 g/10 min after grafting with maleic anhydride while leaving the density and ethylene content unchanged. Conversion of MA to OH or NHR did not alter the MFR any further. The structures of PPE and functional PPEs are given in Fig. 1. The properties of these materials, along with the two types of PMMA studied, are shown in Table 1. PMMA-1 (V825-NA) was provided by Arkema; PMMA-2 was purchased from Aldrich. The zero shear viscosity was measured at 210 °C on a strain-controlled ARES rheometer (TA Instruments) with a 25 mm parallel plate and 1 mm gap. Samples were compression molded (Wabash compression molder) at 210 °C under a pressure of 0.2 MPa for 5 min to 25 mm round disks.

2.2. Synthesis of PPE-g-PMMA

PMMA grafted PPE copolymer (PPE-*g*-PMMA) was synthesized by reversible addition–fragmentation chain transfer polymerization (RAFT) starting from PPE-OH. ACS reagent grade starting materials and solvents were used as received from commercial suppliers without further purification unless otherwise stated. Under an argon atmosphere, $(COCl)_2$ (2.4 mL, 28 mmol) was added by syringe to compound **1** (0.95 g, 2.6 mmol) at room temperature with rapid stirring, causing the vigorous evolution of CO_2(g), CO(g), and HCl(g). It should be noted that corrosive gases were generated during this process. After about 5 h, the evolution of gases ceased and a homogeneous phase was observed. Excess $(COCl)_2$ was removed in vacuo to yield the acyl chloride, **2**. Then 1 g of PPE-OH and 1 g of compound **2** were reacted in 30 mL of toluene at 80 °C to generate compound **3**. The complete conversion of PPE-OH into **3** was confirmed by ^{1}H NMR. 0.3 g of compound **3**, 0.3 g of MMA and 2 mg of AIBN were dissolved into 1 mL of toluene. After the solution was degassed using freeze-pump-thaw cycles, the polymerization was performed at 90 °C for 18 h. The polymer yield was 0.42 g (70%, based on the total materials) and MMA conversion by ^{1}H NMR was determined to be 65%. The product was characterized by ^{1}H NMR and the MMA content was estimated to be 16.8 mol%. The PPE-OH has 4.9 functional groups/chain, thus the average PMMA branch length was estimated to be 64 units. [^{1}H NMR (300 MHz, benzene-d_6): δ = 3.57–3.19 (m, $-O-CH_3$), 2.33–1.85 (m, methylenes from MMA unit), 1.85–0.72 (m, methine, methylene, and methyl groups)].

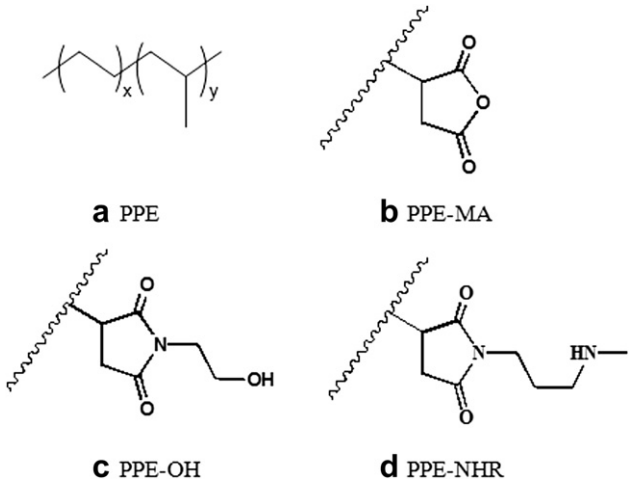

Fig. 1. Structures of the functional polyethylenes used in this study. (a): PPE, poly(propylene-*co*-ethylene) $x/(x + y)$ = (7.3–8) mol%; (b): Succinimide grafted poly(propylene-*co*-ethylene) (PPE-MA); (c): N-(2-hydroxyethyl)-succinimide grafted poly(propylene-*co*-ethylene) (PPE-OH); (d):N-(3-(N-methylamino)-1-propyl)-succinimide grafted poly(propylene-*co*-ethylene) (PPE-NHR). The wiggly lines in (b), (c), (d) represent poly(propylene-*co*-ethylene) backbones.

2.2.1. Preparation of PPE-X/PMMA blends (X = MA, OH, NHR)

PPE-X/PMMA blends were prepared in a recirculating, conical twin screw extruder (DACA Instruments, 4 g capacity) at 200 rpm and temperature of 210 °C with nitrogen purge. After mixing for 5 min, the blends were extruded and collected.

2.3. Characterization

2.3.1. Nano-indentation test

Nano-indentation was performed using a Nano Indenter (MTS Systems Co.). The indentation load-displacement behavior of PMMA, PPE materials and their blends were tested with a Berkovich indenter tip to determine hardness and elastic modulus. The

Table 1
Molecular characteristics of polymers used.

Sample	Mn (kg/mol)	Mw (kg/mol)	PDI	T_m[a] (°C)	η_0[b] (Pa s)
PPE-MA[c]	49.8	92.7	1.86	55	1.3×10^2
PPE-OH[c]	61.0	104.6	1.71	55	1.7×10^2
PPE-NHR[c]	63.1	108.4	1.72	55	1.9×10^2
PPE				64	3.9×10^2
PMMA-1[d]	63.3	92.7	1.46	–	2.5×10^4
PMMA-2[d]	9.53	15.4	1.62	–	0.8×10^2
PPE-*g*-PMMA[c]	72.2	238.6	3.30	–	–

[a] Onset of melting.
[b] Zero shear viscosity measured at 210 °C.
[c] Molecular weights measured by high temperature GPC at 160 °C.
[d] Molecular weights measured by GPC at room temperature using polystyrene standards.

samples were films made by compression molding with thickness ~1 mm and mounted on an Al puck with cyano acrylate adhesive (Superglue, Locktite). The approaching velocity and the harmonic displacement of the nano-indentation tip toward a target surface were maintained at 10 nm/s ± 0.2 nm/s and 2 nm respectively for all the testing surfaces.

2.3.2. Nano-scratch test

The scratch test was performed using the same Nano Indenter instrument as above with a different tip. A diamond indenter with 90° conical geometry was used. In the scratch test, a normal force was applied on the surface at a constant rate of increase as the indenter moves a certain distance laterally, progressively increasing the applied load from 0 to 40 mN. After the scratch test, images of the scratched surface were obtained with an optical microscope. All operation parameters are summarized in Table 2.

Three scratches (separated by at least 1 mm) were created on each sample to avoid errors due to point defects on the surface. As the indenter moved laterally on the surface, penetration depth versus scratch distance was recorded to evaluate scratch resistance. After each test the indenter traversed the scratch area again while applying minimum load to record the surface contours. By comparing the profiles during and after scratching, changes in depth on the scratched surface can be detected.

2.3.3. Scanning electron microscopy (SEM)

SEM images were taken with a JEOL 6500 scanning electron microscope with a field-emission gun. Polymer blends were quenched and fractured in liquid nitrogen immediately after extrusion to preserve morphology. All SEM samples were then sputter coated with platinum to a thickness of approximately 75 Å to make them conductive. The particle size (Table 4) was determined by measuring ~100 diameters manually.

2.3.4. Tensile test

A MINIMAT tensile tester (Rheometric Scientific) with an extension rate of 1 mm/s was used to investigate the tensile properties of the blends. Functional PPE/PMMA-1 were molded into dogbone samples (12 mm gage length, 0.5 mm gage thickness, 3 mm gage width) by compression molding from pellets at 210 °C under 0.2 MPa between two polytetrafluoroethylene (PTFE) coated aluminum foils (Saint-Gobain Performance Plastics). They were dried in a vacuum oven at room temperature over night before testing.

2.3.5. Differential scanning calorimetry (DSC)

Differential scanning calorimetry was performed on a TA DSC Q1000 utilizing an indium standard for temperature calibration. At least 4 mg of sample contained in hermetically sealed aluminum pans were analyzed under N_2 with a 10 °C/min heating rate. Thermal transition temperatures were determined from a second heating scan, after annealing above the glass transition or melting point for at least 1 min to erase thermal history.

2.3.6. High temperature gel permeation chromatography

The high temperature GPC system PL-GPC 220 (Agilent Systems) was used to measure the molecular weights and distribution of PPE materials. Trichlorobenzene with 0.0125 wt% of butylated hydroxytoluene was used as eluent phase with flow rate 1.0 mL/min at 135 °C. The data were analyzed against a polystyrene standard calibration using the following Mark–Houwink parameters: polystyrene in TCB: $K = 12.1 \times 10^{-5}$ $\alpha = 0.707$; polypropylene in TCB: $K = 19.0 \times 10^{-5}$ $\alpha = 0.725$.

Table 2
Parameters for nano-scratch test.

Parameter	Quantity
Scratch length	500 μm
Scratch velocity	10.000 μm/s
Starting scratching load	0.000 mN
Maximum scratch load	40.000 mN
Profiling and scratch acquisition rate	5.000 Hz

Table 3
Modulus and hardness determined from nano-indentation tests.

Sample	Modulus (MPa)	Hardness (MPa)
PPE	43 ± 4	6 ± 0.5
PPE/ PMMA-1 (70/30)	57 ± 6	8 ± 1.1
PPE-MA	49 ± 5	8 ± 0.7
PPE-MA/ PMMA-1 (70/30)	94 ± 4	13 ± 1.2
PPE-OH	46 ± 3	7 ± 0.6
PPE-OH/ PMMA-1 (70/30)	98 ± 5	14 ± 1.5
PPE-NHR	45 ± 4	6 ± 0.6
PPE-NHR/ PMMA-1 (70/30)	113 ± 8	18 ± 1.7
PMMA-1	$(4.3 \pm 0.2) \times 10^3$	$(2.6 \pm 0.1) \times 10^2$
PMMA-2	$(1.5 \pm 0.3) \times 10^3$	40 ± 5

2.3.7. Adhesion test

In order to test the capabilities of functional PPEs and PPE-*g*-PMMA as adhesion promoters, they were laminated between PPE and PMMA, and annealed at 180 °C. The adhesion between PPE and PMMA was then tested. The functional PPEs and PPE-*g*-PMMA were dissolved in benzene at 80 °C (0.03g/13 mL), and then the temperature of the solution was lowered to 50 °C. Premade PMMA films were dipped into the solution for 5 s and then dried in fume hood. Then the coated PMMA film and a premade PPE film were pressed into intimate contact (sandwiched between polytetrafluoroethylene (PTFE)-coated aluminum foil) and laminated for 100 s at 180 °C under 0.1 MPa pressure. The bilayer samples were cooled by water to room temperature. The 180° peel tests were performed on the same MINIMAT Tensile tester at an extension rate of 0.33 mm/s and a total travel distance of 50 mm.

3. Results and discussion

3.1. Nano-indentation and nano-scratch tests

We blended PMMA-1 with PPE and three types of functional PPEs, namely maleic anhydride grafted PPE (PPE-MA), hydroxyl group grafted PPE (PPE-OH) and secondary amine group grafted PPE (PPE-NHR). Then we evaluated the mechanical properties and compatibility of resulting blends by using nano-indentation tests, nano-scratch tests, tensile tests, rheological characterization, SEM and peel adhesion tests.

Table 4
Average particle size for different blends.

Blend	$<d_s>$[a] (μm)	$<d_s>/<d_n>$[b]
10/90 blend		
PPE/ PMMA-1	1.93	1.58
PPE-MA/ PMMA-1	1.27	1.48
PPE-OH/ PMMA-1	0.91	1.45
PPE-NHR/ PMMA-1	0.69	1.37
90/10 blend		
PPE/PMMA-1	20.3	1.64
PPE-MA/ PMMA-1	10.6	1.43
PPE-OH/ PMMA-1	8.9	1.38
PPE-NHR/ PMMA-1	6.9	1.36
PPE/ PMMA-2	1.94	1.34
PPE-NHR/ PMMA-2	0.51	1.13

[a] $\langle d_S \rangle$: Surface area average diameter; $\langle d_S \rangle = \sum d_i^3 / \sum d_i^2$.
[b] $\langle d_n \rangle$: Number average particle size; $\langle d_n \rangle = \sum n_i d_i / \sum n_i$.

In a nano-indentation test [13–18], an indenter tip is driven into the sample by applying an increasing load up to some preset value. The load is then decreased until partial or complete relaxation occurs. The Young's modulus of PMMA-1 was determined to be 4.3 GPa. When it was blended into various PPE materials (as shown in Table 3), non-modified PPE only had a slight increase of modulus and hardness. However, for all the modified PPEs, the modulus and hardness increased significantly via blending with PMMA compared with the PPEs without PMMA. We attribute this behavior to the interfacial bonding between PMMA and complementary functional groups on the modified PPE backbones. The rigid PMMA particles provide enormous resistance to tensile force as the Young's modulus of PMMA is several orders of magnitude higher than that of the PPE materials. PPE-NHR gave the best improvement, almost three times higher, suggesting the highest reactivity of secondary amine towards the PMMA ester group among the three functionalities.

For the nano-scratch test [19–25], the normal force increased linearly with scratch distance up to 40 mN as the indenter moves laterally on the surfaces to be tested (Fig. 2a). All the single unblended PPE materials show very similar resistance to the normal force. Penetration depth increases linearly with force for PPE and functionalized PPE materials. However, dramatic changes were observed after PMMA was blended. Even with a weak interfacial interaction, PPE/PMMA-1 presents a significant resistance to the scratching normal force. Starting from scratch distance ~250 μm, the indenter could no longer penetrate into the material even with increased forces. Instead, the indenter's vertical decent was stalled after 250 μm. It is remarkable that functional PPEs generated even more scratch resistance, in the following order: PPE-NHR > PPE-OH > PPE-MA.

It is surprising that the blend PPE-NHR/PMMA-2 (70/30) did not generate as strong scratch resistance as PPE-NHR/PMMA-1 (70/30), where higher molecular weight PMMA-1 was used. Although lower molecular weight PMMA-2 matched PPE viscosities and gave rise to much finer morphology, its modulus and especially hardness are much lower as shown in Table 3. This is because the molecular weight of PMMA-2 is lower than the PMMA entanglement molecular weight and is therefore much more brittle than PMMA-1.

Fig. 3 presents an example of how the scratch appearance is changed with the addition of PMMA. The scratch in PPE-NHR is much more visible than in PPE-NHR/PMMA blends. In PPE-NHR there was an obvious pile up of material while the scratch of blends was narrower at the start of the scratch and smeared at surface when the force increased.

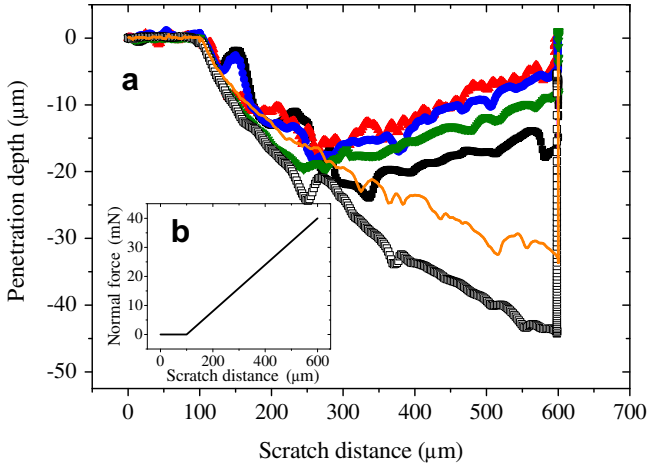

Fig. 2. (a) Penetration depth vs. scratch distance in nano-scratch tests for different materials. ▲: PPE-NHR/PMMA-1 (70/30); ● : PPE-OH/PMMA-1 (70/30); ◆: PPE-MA/PMMA-1 (70/30); ■: PPE/PMMA-1 (70/30); ——: PPE-NHR/PMMA-2 (70/30); □: PPE (Note the penetration curve of PPE nearly overlapped with PPE-NHR, PPE-OH and PPE-MA.) (b) For all samples the applied normal force was increased linearly as the indenter moved laterally.

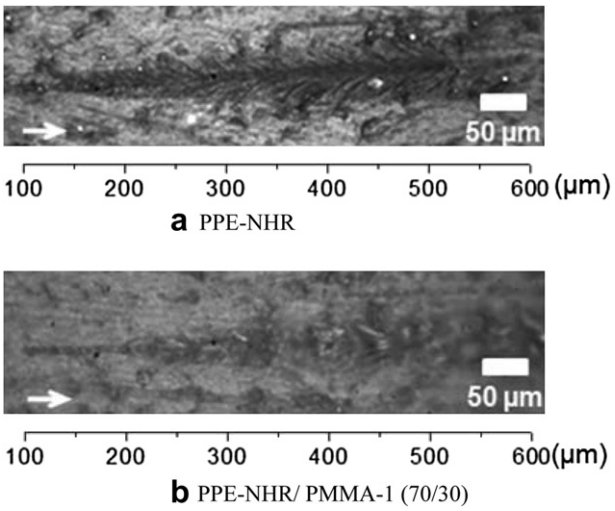

Fig. 3. (a) Optical micrograph of a scratch path on PPE-NHR; (b) The scratch path on PPE-NHR/PMMA-1 blend (70/30) is less visible. Arrows indicate the scratch direction.

Stress vs. elongation data are shown in Fig. 4. They confirm the ranking from nano-indentation and nano-scratch tests. While the ultimate elongation of all PPE materials falls beyond the instrument limitation, the blends also showed significant elongation. PPE-NHR, again, gave the best improvement in terms of ultimate elongation and elastic modulus, followed by PPE-OH, PPE-MA and non-modified PPE. It is quite remarkable that the stress at 100% elongation for PPE-NHR/PMMA-1 blend surpassed the other blends by more than 50% and was even 30% larger than the matrix, PPE-NHR.

Xiang et al. [26] studied scratch behavior of a broad range of polymers to understand how the material characteristics affect scratch resistance. They found that tensile tear is responsible for the brittle fracture mode during scratch, especially for brittle materials, which leads to cracks and crazes. However, for elastomers used in our research, shear yielding is the dominant factor resulting in scratch damage. For shear yielding, modulus, yield stress and friction coefficient determine the scratch resistance. Obviously, increased modulus and yield stress of the modified PPE/PMMA blends lead to better shear yielding resistance. As a result, scratch

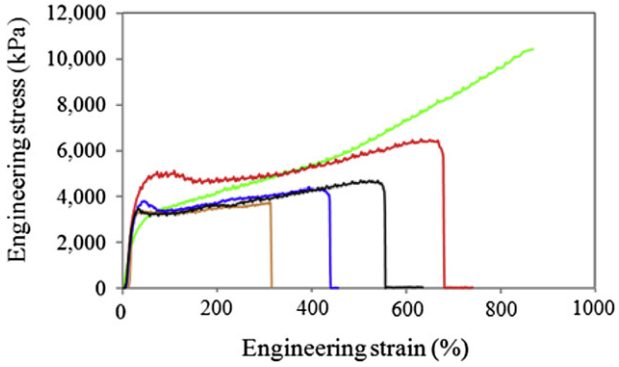

Fig. 4. Engineering stress vs. engineering strain for PPE, functional PPEs and their blends with PMMA-1. ——: PPE; (Note the stress–strain curve of PPE nearly overlapped with PPE-NHR, PPE-OH and PPE-MA.) ——: PPE-NHR/PMMA-1 (70/30); ——: PPE-OH/PMMA-1 (70/30); ——: PPE-MA/PMMA-1 (70/30); ——: PPE/PMMA-1 (70/30).

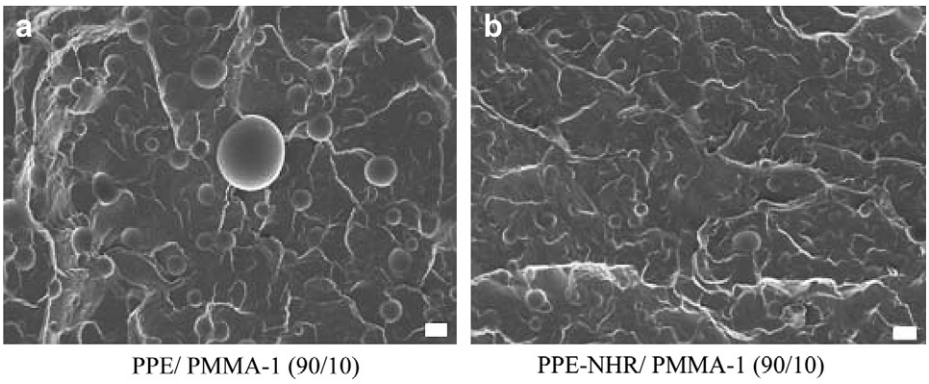

Fig. 5. SEM micro-photographs of cryogenically fractured surfaces. (a) Blend of PPE/PMMA-1 (90/10); (b) Blend of PPE-NHR/PMMA-1 (90/10). Scale bar represents 10 μm.

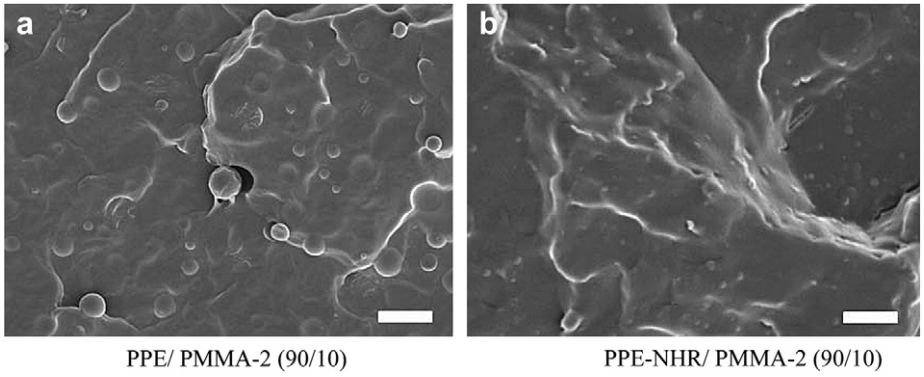

Fig. 6. SEM micro-photographs of cryogenically fractured surfaces. (a) Blend of PPE/PMMA-2 (90/10); (b) Blend of PPE-NHR/PMMA-2 (90/10). Scale bar represents 5 μm.

resistance of PPE and functionalized PPEs were increased after blending PMMA.

3.2. Blend morphology

PPE-X and PMMA blended at 90/10 and 10/90 weight ratio generated droplets of one phase dispersed in the other. Figs. 5 and 6 present the morphology of blends with PMMAs of different molecular weights. Surface average particle size along with size distribution is provided in Table 4. With PMMA-1 as the continuous phase, PPE drop size is much smaller because its viscosity is nearly 100 times smaller. In both blends particle size decreased the same order as adhesion increased: PPE > PPE-MA > PPE-OH > PPE-NHR.

Compared with non-modified PPE, although PPE-NHR showed dramatically improved scratch resistance and reduced particle diameter, the average particle size still remained at about 5 μm when blended with PMMA-1 [27]. When blended with low molecular weight PMMA-2, particle size decreased dramatically (as shown in Table 4). Yet, as discussed above, the scratch resistance

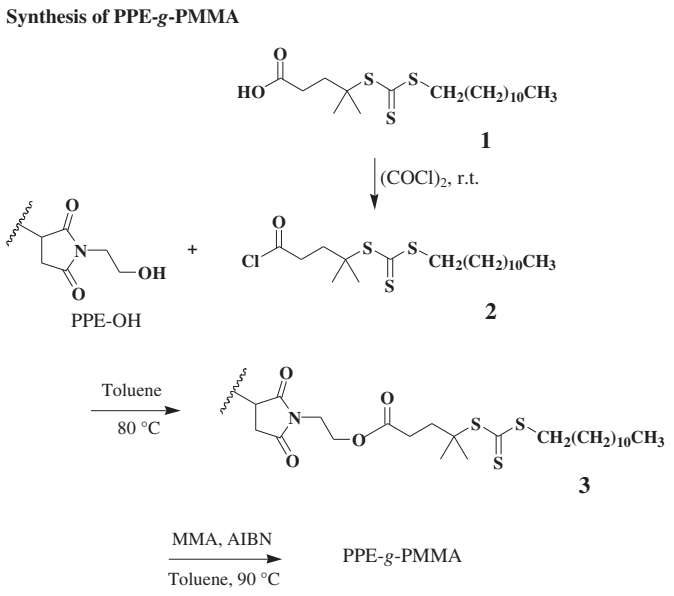

Scheme 1. Synthesis of PMMA grafted PPE (PPE-*g*-PMMA) from PPE-OH.

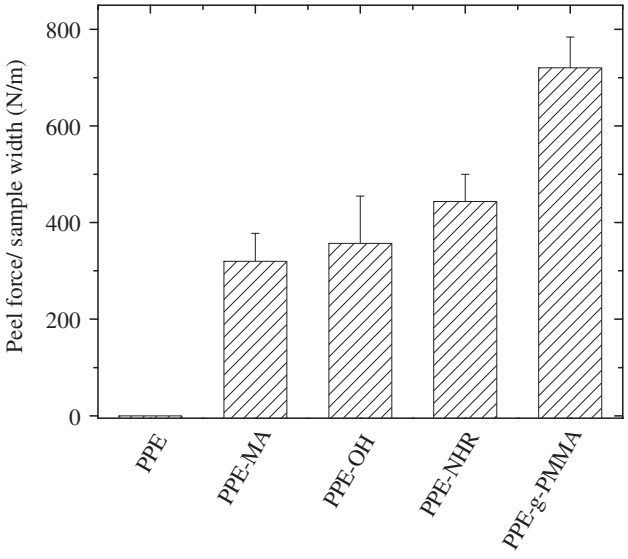

Fig. 7. Peel force/sample width for adhesion between PPE and PMMA. PPE-g-PMMA and the functional PPEs were coated on the PMMA and then the films were laminated at 180 °C.

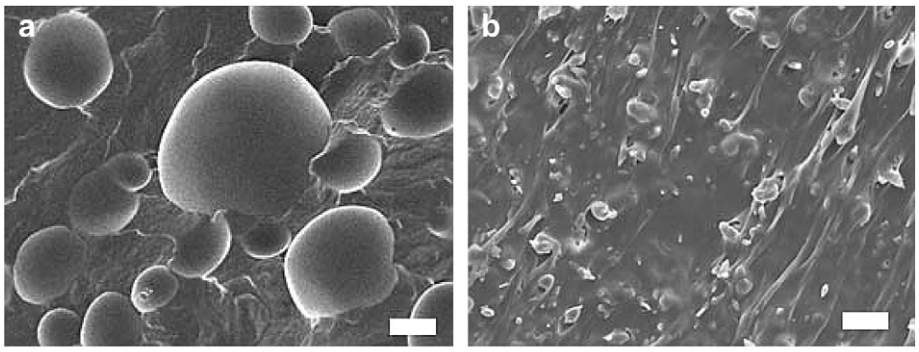

Fig. 8. SEM micro-photographs of cryogenically fractured surfaces. (a) Blend of PPE/PMMA-1 (70/30); (b) Blend of PPE/PMMA-1/PPE-*g*-PMMA (67/28/5). Scale bar represents 10 μm.

was not better. For instance, in Fig. 2, with the same amount of PMMA added into PPE-NHR, PMMA-1 blend showed significantly better scratch resistance than PMMA-2 blend. This is because the molecular weight of PMMA-2 was lower than PMMA entanglement molecular weight and its mechanical properties were inferior to PMMA-1 (as shown in Table 3). The blends with high molecular weight PMMA exhibit better scratch resistance despite having bigger particle size.

3.3. The application of PPE-g-PMMA

With the success we have in the blend of functional PPEs and PMMA, we explored the effect of a premade graft copolymer on adhesion and particle size. As shown in Scheme 1, starting from PPE-OH, we grafted PMMA onto PPE backbones to obtain PMMA grafted PPE (PPE-*g*-PMMA). As shown in Table 1, the molecular weight of this graft copolymer and polydispersity increased significantly compared to the starting PPE-OH.

Fig. 7 illustrates that PPE-g-PMMA greatly increased the adhesion between PPE and PMMA. The adhesion between non-modified PPE and PMMA was almost zero as expected. Due to the immiscibility of these two polymers, there is very limited amount of entanglement achieved between them leading to very weak adhesion. Nonetheless, when PPE-MA, PPE-OH and PPE-NHR were coated, adhesion between PPE and PMMA increased significantly to around 400 N/m. PPE-NHR, again, gave the best improvement among the three functional groups suggesting the best reactivity. It is remarkable that the PPE-*g*-PMMA copolymer generated at least 700 N/m peel strength between PPE and PMMA in contrast with other functional PPEs.

PPE and PMMA-1 were blended at 70/30 weight ratio. Due to the immiscibility between polyolefin and PMMA and the high viscosity of PMMA-1, the PPE/PMMA-1 blend had a number average particle size above 20 μm as shown in Fig. 8(a). However, when PPE-*g*-PMMA was blended into PPE/PMMA-1, the particle size dropped significantly as shown in Fig. 8(b). We attribute the particle size reduction of the dispersed phase to the stabilization of blend morphology by the PPE-*g*-PMMA copolymer at the interface during melt blending. The graft copolymer is expected to stabilize the small particle size by reducing the interfacial tension and thus giving rise to a reduced coalescence rate.

4. Conclusion

Although conventional polyolefin and PMMA blends are highly incompatible, we improved compatibility and adhesion between them by reactive compatibilization with functional polyolefins. The compatibility of a poly(propylene-co-ethylene), PPE and three functional PPEs with PMMA ranked in a decreasing order as follows: PPE-NHR > PPE-OH > PPE-MA > PPE using mechanical (nano-indentation, nano-scratch and tensile tests), morphological (scanning electron microscopy with image analysis, particle size analysis) and adhesion tests. Secondary amine gave the best improvement, suggestive of highest reactivity with the ester group on PMMA. We obtained the greatest improvement in adhesion using a synthesized PMMA grafted PPE copolymer.

Acknowledgments

This work was supported by The Dow Chemical Company. Parts of this work were carried out in the Characterization Facility, University of Minnesota, which receives partial support from NSF through the MRSEC program.

References

[1] Kobayashi S, Song J, Silvis HC, Macosko CW, Hillmyer MA. Ind Eng Chem Res 2011;50(6):3274–9.
[2] Song J, Ewoldt RH, Hu W, Silvis HC, Macosko CW. AIChE J 2011;57(12):3496–506.
[3] Boaen NK, Hillmyer MA. Chem Soc Rev 2005;34(3):267–75.
[4] Chung TC. Functionalization of polyolefins. Academic Press; 2002.
[5] Song J, Batra A, Rego MJ, Macosko CW. Prog Org Coat 2011;72(3):492–7.
[6] Stutz H, Heckmann W, Pötschke P, Wallheinke K. J Appl Polym Sci 2002; 83(13):2901–5.
[7] Schneider Y, Azoulay JD, Coffin RC, Bazan GC. J Am Chem Soc 2008;130(28): 10464–5.
[8] Kaneyoshi H, I Y, Matyjaszewski K. Macromolecules 2005;38(20):8163–9.
[9] Kaneko H, Kojoh S-I, Kawahara N, Matsuo S, Matsugi T, Kashiwa N. J Polym Sci Part A 2005;43(21):5103–18.
[10] Harrats CB, Benabdallah T, Groeninckx G, Jerome R. J Polym Sci Part B 2005; 43(1):22–34.
[11] Yoshihara S, Maekawa K, Uno M. 2001247723 Japan 2001.
[12] Silvis CH, Hahn SF, Pawlowski DF, Ansems P, Mergenhagen LK, Lakrout H. WO 2008/080081.
[13] Consiglio R, Randall NX, Bellaton B, von Stebut J. Thin Solid Films 1998; 332(1–2):151–6.
[14] Oliver WC, Pharr GM. J Mater Res 2004;19(1):3–20.
[15] Lee C, Wei X, Kysar JW, Hone J. Science 2008;321(5887):385–8.
[16] Hodzic A, Stachurski ZH, Kim JK. Polymer 2000;41(18):6895–905.
[17] Munz M, Sturm H, Stark W. Polymer 2005;46(21):9097–112.
[18] Soloukhin VA, Posthumus W, Brokken-Zijp JCM, Loos J, de With G. Polymer 2002;43(23):6169–81.
[19] Bauer F, Ernst H, Decker U, Findeisen M, Glasel HJ, Langguth H, et al. Macromol Chem Phys 2000;201(18):2654–9.
[20] Fang TH, Weng CI, Chang JG. Nanotechnology 2000;11(3):181–7.
[21] Malzbender J, den Toonder JMJ, Balkenende AR, de With G. Mater Sci Engn R 2002;36(2–3):47–103.
[22] Zhou SX, Wu LM, Sun J, Shen WD. Prog Org Coat 2002;45(1):33–42.
[23] Brostow W, Kovacevic V, Vrsaljko D, Whitworth J. J Mater Educ 2010;32(5–6): 273–90.
[24] Chen SW, You B, Zhou SX, Wu LM. J Appl Polym Sci 2009;112(6):3634–9.
[25] Li LQ, Hirtz M, Wang WC, Du CA, Fuchs H, Chi LF. Adv Mater 2010;22(12): 1374–8.
[26] Xiang C, Sue HJ, Chu J, Coleman BJ. Polym Sci. Part B Polym Phys 2001;39(1):47–59.
[27] Vleminckx G, Bose S, Leys J, Vermant J, Wubbenhorst M, Abdala AA, et al. ACS Appl Mater Interfaces 2011;3(8):3172–80.